Mechanics of Materials 70 (2014) 1–17

Contents lists available at ScienceDirect

Mechanics of Materials

journal homepage: www.elsevier.com/locate/mechmat

Mechanical modeling of incompressible particle-reinforced neo-Hookean composites based on numerical homogenization

Zaoyang Guo [a,b,*], Xiaohao Shi [c], Yang Chen [b], Huapeng Chen [d], Xiongqi Peng [e,*], Philip Harrison [f]

[a] State Key Laboratory of Coal Mine Disaster Dynamics and Control, Chongqing University, Chongqing 400044, China
[b] Department of Engineering Mechanics, Chongqing University, Chongqing 400044, China
[c] Institute of Biomedical Engineering and Health Sciences, Changzhou University, Changzhou, Jiangsu 213164, China
[d] School of Engineering, University of Greenwich, Chatham Maritime, Kent ME4 4TB, UK
[e] Department of Plasticity Technology, Shanghai Jiao Tong University, Shanghai 200030, China
[f] School of Engineering, University of Glasgow, Glasgow G12 8QQ, UK

ARTICLE INFO

Article history:
Received 1 May 2013
Received in revised form 6 October 2013
Available online 4 December 2013

Keywords:
Particle-reinforced composite
Representative volume element (RVE)
Neo-Hookean
Numerical homogenization
Hyperelasticity

ABSTRACT

In this paper, the mechanical response of incompressible particle-reinforced neo-Hookean composites (IPRNC) under general finite deformations is investigated numerically. Three-dimensional Representative Volume Element (RVE) models containing 27 non-overlapping identical randomly distributed spheres are created to represent neo-Hookean composites consisting of incompressible neo-Hookean elastomeric spheres embedded within another incompressible neo-Hookean elastomeric matrix. Four types of finite deformation (i.e., uniaxial tension, uniaxial compression, simple shear and general biaxial deformation) are simulated using the finite element method (FEM) and the RVE models with periodic boundary condition (PBC) enforced. The simulation results show that the overall mechanical response of the IPRNC can be well-predicted by another simple incompressible neo-Hookean model up to the deformation the FEM simulation can reach. It is also shown that the effective shear modulus of the IPRNC can be well-predicted as a function of both particle volume fraction and particle/matrix stiffness ratio, using the classical linear elastic estimation within the limit of current FEM software.

1. Introduction

A fundamental problem for particle-reinforced composites (PRC) is to predict the overall mechanical behavior of the composite based on the mechanical properties of the constituents and the microstructure of the composites. Guth (1945) extended Einstein's linear estimate originally developed for viscous fluid and proposed a second order polynomial to predict the small strain Young's modulus of (rigid) particle-filled solids. Kerner (1956) designed an averaging procedure to estimate the effective shear modulus and bulk modulus of the PRC. Hill (1965) proposed a self-consistent model to estimate the effective shear modulus of the PRC. The three-phase model developed by Christensen and Lo (1979) gives a very good prediction of the PRCs effective shear modulus (Segurado and Llorca, 2002). Torquato (1998) derived accurate expressions for the bulk and shear moduli of the PRC based on a third-order approximation. Although a few studies investigated some special microstructures such as cubic arrays of spheres (e.g., Cohen, 2004), most papers in the literature have focused on macroscopically isotropic composites

* Corresponding authors. Address: State Key Laboratory of Coal Mine Disaster Dynamics and Control, Chongqing University, Chongqing 400044, China. Tel.: +86 13983897097 (Z. Guo).
E-mail addresses: zyguo01@gmail.com (Z. Guo), xqpeng@sjtu.edu.cn (X. Peng).

http://dx.doi.org/10.1016/j.mechmat.2013.11.004
0167-6636/

with randomly distributed particles. Besides the direct estimation of the effective moduli of the PRC, some rigorous bounds for the elastic properties of the PRC have been obtained from variational principles (e.g., Hashin and Shtrikman, 1963). Another approach to investigate the "overall" mechanical behavior of the PRC is to solve the boundary value problems for a representative volume element (RVE) model of the composite numerically (Michel et al., 1999). Drugan and Willis (1996) showed that a small size RVE model can predict accurately the mechanical response of the PRC. Segurado and Llorca (2002) provided a comprehensive numerical study of the mechanical properties of the linear elastic PRC using multi-particle RVE models.

Although the mechanical properties of the PRC in infinitesimal strain have been investigated extensively, their mechanical behavior in the finite deformation regime is still not well-understood due to the intrinsic difficulties related to the geometrical and material nonlinearities. Hill (1972) proposed a set of macroscopic variables for constitutive modeling of composites in finite deformation. Based on that, Ogden (1974) derived an approximate expression for the overall bulk modulus of the PRC with second-order isotropic compressible elastic constituents under finite strain. Hashin (1985) studied the response of hyperelastic PRC under hydrostatic loading. Imam et al. (1995) derived the second order elastic field for incompressible hyperelastic composites with dilute inclusions, which was then employed to estimate the overall moduli of the PRC. Although recently several research groups have investigated hyperelastic composites with inclusions in two dimension (which physically implies composites with aligned fiber reinforcement) and some related boundary value problems are solved analytically (e.g., deBotton et al., 2006; Guo et al., 2008; Guo et al., 2006; Lopez-Pamies, 2010), analytical solutions for three-dimensional PRC model under general homogeneous displacement boundary conditions are far more difficult. Castaneda (1989) proposed a self-consistent approach to predict the shear modulus of incompressible particle-reinforced neo-Hookean composites (IPRNC). Bergstrom and Boyce (1999) used the concept of strain amplification under large strain to estimate the shear modulus of incompressible neo-Hookean composites filled with rigid particles. Because these two models are not based on an accurate approximation of the elastic fields, it is not surprising to find that they don't provide good estimates of effective shear modulus of IPRNC with moderate particle volume fractions. Recently Avazmohammadi and Castaneda (2012) developed a tangent second-order (TSO) method to investigate the macroscopic response of PRC in finite deformation and an explicit formula is derived to approximate the strain energy of incompressible neo-Hookean composites reinforced with rigid particles.

The numerical studies of hyperelastic composites available in the literature are also mainly limited to two-dimensional problems of composites with aligned fibers or voids (e.g., Guo et al., 2008; Moraleda et al., 2007, 2009; Tang et al., 2012a, b), though Bergstrom and Boyce (1999) used simple 2D axisymmetric models to simulate IPRNC under uniaxial deformation. Three-dimensional RVE modeling in finite deformation is only investigated for single-fiber unit cell (Guo et al., 2007). To the best of the authors' knowledge, there is no comprehensive numerical study of the PRC under finite deformation published in the literature.

Because it is difficult to predict the mechanical response of the PRC under general finite deformation theoretically due to the related geometrical and material nonlinearities, this study employs the numerical homogenization approach to investigate the mechanical behavior of the simplest hyperelastic PRC under general finite deformation, in which the mechanical properties of both the matrix and the reinforcement are described by an incompressible neo-Hookean model respectively. In this paper, three-dimensional RVE models are created to represent the neo-Hookean composite which consists of one incompressible neo-Hookean elastomer embedded with another randomly distributed equal-sized spherical incompressible neo-Hookean particle reinforcement. Commercial finite element analysis software ABAQUS is employed for the numerical simulations of the RVE models. Periodic boundary conditions (PBC) are implemented in the RVE models when general finite deformation is applied to the RVE models. The numerical results show that the overall mechanical responses of the IPRNC can be well predicted by another simple incompressible neo-Hookean model. The simulation results also suggest that the classical linear elastic estimation (Christensen and Lo, 1979) can be used to predict the effective shear modulus of the IPRNC with different particle volume fraction and different particle/matrix stiffness ratio.

The structure of the paper is as follows: In Section 2, the IPRNC to be investigated is described and the theoretical basis of the numerical homogenization in finite deformation (Hill, 1972; Ogden, 1974) is also introduced. In Section 3, the RVE models are developed for numerical simulations using finite element method (FEM) and some related issues (e.g., isotropy of the RVE models, FEM mesh) are discussed. The results of the RVE simulations are presented and investigated in Section 4. The effective modulus of the hyperelastic composites is also compared with classical linear elastic estimation. Some concluding remarks are given in Section 5.

2. Particle-reinforced neo-Hookean composites and theoretical basis of numerical homogenization

First of all, some basic concepts in continuum mechanics need to be introduced. For a continuum solid, the deformation gradient is defined as $\mathbf{F} = \partial \mathbf{x}/\partial \mathbf{X}$, where $\mathbf{X}$ and $\mathbf{x}$ denote the positions of a typical material point respectively in the original (undeformed) and deformed configuration of the solid, respectively. The mechanical behavior of an isotropic hyperelastic material can be determined by its strain energy function (per unit volume in the original configuration) $W = W(\mathbf{F})$. If the material is compressible, the nominal stress $\mathbf{P}$ can be obtained as

$$\mathbf{P} = \frac{\partial W(\mathbf{F})}{\partial \mathbf{F}}, \quad P_{ij} = \frac{\partial W}{\partial F_{ij}}, \tag{1}$$

while for an incompressible material, it reads

$$\mathbf{P} = -p\mathbf{F}^{-T} + \frac{\partial W(\mathbf{F})}{\partial \mathbf{F}}, \tag{2}$$

where p is the (arbitrary) pressure. The simplest model for hyperelastic materials is the incompressible neo-Hookean model, as follows:

$$W(\mathbf{F}) = \frac{1}{2}\mu(I_1 - 3), \tag{3}$$

where the only material constant μ is the shear modulus of the material; $I_1 = tr(\mathbf{C})$ is the first invariant of the right Cauchy-Green deformation tensor $\mathbf{C} = \mathbf{F}^T\mathbf{F}$.

In the paper, our interest will focus on the mechanical behavior of the simplest hyperelastic PRC, the so-called "incompressible particle-reinforced neo-Hookean composite" (IPRNC), in which both the matrix and the particle reinforcement are incompressible neo-Hookean materials and they are perfectly bonded at the surfaces. Let μ_m and μ_r denote the shear moduli of the matrix and the reinforcement respectively. If the mechanical properties of the composite are assumed to be macroscopically isotropic and homogeneous, only two parameters, the stiffness ratio μ_r/μ_m and the volume fraction of the reinforcement c, need to be considered. Hence the shear modulus of the matrix μ_m can be set as 1 (one unit) without losing any generality.

The macroscopic mechanical behavior of the (microscopically inhomogeneous) hyperelastic composite can be characterized by the constitutive macro-variables defined in Hill (1972). We now consider a representative volume of the inhomogeneous hyperelastic material which occupies volume V in the original configuration. The volume average (denoted by an over-bar) of the deformation gradient $\mathbf{F}$, the nominal stress tensor $\mathbf{P}$, and the strain energy W are given by (Hill, 1972; Ogden, 1974)

$$\bar{\mathbf{F}} = \frac{\int_V \mathbf{F}dV}{V}, \quad \bar{\mathbf{P}} = \frac{\int_V \mathbf{P}dV}{V}, \quad \overline{W(\mathbf{F})} = \frac{\int_V W(\mathbf{F})dV}{V}. \tag{4}$$

Using the equilibrium equations and the divergence theorem, it can be derived that

$$\bar{F}_{ij} = \frac{\int_S x_i n_j dS}{V}, \tag{5}$$

where S is the surface of the volume V; $\mathbf{n} = n_j\mathbf{e}_j$ is the outward unit vector normal to the surface S. Here $\mathbf{e}_j$ is the unit vector in the direction of the X_j axis. This means that the average deformation gradient $\bar{\mathbf{F}}$ can be computed in terms of the displacement on the surface S. Similarly, if the continuum body is in equilibrium, the average nominal stress $\bar{\mathbf{P}}$ can be obtained as

$$\bar{P}_{ij} = \frac{\int_S X_i P_{kj} n_k dS}{V}, \tag{6}$$

which implies that the average nominal stress $\bar{\mathbf{P}}$ can be computed in terms of the nominal stress $\mathbf{P}$ on the surface S. Hill (1972) showed that

$$\bar{\mathbf{P}} = \frac{\partial \overline{W(\mathbf{F})}}{\partial \bar{\mathbf{F}}} \tag{7}$$

for compressible composites. If the material is incompressible, it reads

$$\bar{\mathbf{P}} = -p\bar{\mathbf{F}}^{-T} + \frac{\partial \overline{W(\mathbf{F})}}{\partial \bar{\mathbf{F}}}, \tag{8}$$

Hence $\overline{W(\mathbf{F})}$ can be treated as a potential (strain energy) for the volume V and a function of $\bar{\mathbf{F}}$. The mechanical behavior of the overall composite can be determined by $\overline{W} \equiv \overline{W}(\bar{\mathbf{F}})$. However, because of the fundamental difficulties caused by the related geometrical and material nonlinearity, even for the simplest PRC defined above, it is still very difficult (if not impossible) to derive an analytical expression for the strain energy field in the volume V under a general deformation state (e.g., the explicit strain energy approximation obtained in (Avazmohammadi and Castaneda, 2012) for incompressible neo-Hookean composite with rigid reinforcement has about 200 terms).

To overcome the theoretical difficulty, numerical homogenization methods have been proposed to estimate the effective properties of microscopically inhomogeneous composites (Kouznetesova, 2002; Michel et al., 1999). Based on the macro-variables defined in Hill (1972), to determine the mechanical behavior of hyperelastic composites, for any given "overall" deformation (represented by the average deformation gradient $\bar{\mathbf{F}}$), appropriate displacement boundary conditions which satisfy (5) are applied to a geometrical representative model and the corresponding stress/strain fields can then be computed numerically (usually by FEM). The macroscopically defined nominal stress tensor $\bar{\mathbf{P}}$ can then be obtained from (7) and the related strain energy $\overline{W}(\bar{\mathbf{F}})$ can also be computed numerically. For macroscopically homogeneous and isotropic incompressible hyperelastic material, any general deformation can be treated as a biaxial deformation in its principal directions. Hence any general deformation can be represented by principal stretches λ_1 and λ_2 (the third principal stretch can be determined by the incompressibility constraint as $\lambda_3 = 1/(\lambda_1\lambda_2)$). If the principal stretches are further sorted as $\lambda_1 \geqslant \lambda_2 \geqslant \lambda_3$, then only the region $\{(\lambda_1, \lambda_2) | \lambda_1 \geqslant 1, \lambda_1 \geqslant \lambda_2 \geqslant \lambda_1^{-1/2}\}$ needs to be investigated numerically. Now the overall strain energy function can be written as $\overline{W} \equiv \overline{W}(\lambda_1, \lambda_2)$. When the invariant approach is used, the overall strain energy function can be represented as $\overline{W} \equiv \overline{W}(I_1, I_2)$, where $I_2 = \frac{1}{2}[(tr\mathbf{C})^2 - tr\mathbf{C}^2]$ is the second invariant of the right Cauchy-Green deformation tensor $\mathbf{C}$. If sufficient values of $\overline{W}$ are computed numerically, for some simple composites, the data might suggest a simple function $\overline{W}(\lambda_1, \lambda_2)$ or $\overline{W}(I_1, I_2)$, as illustrated later in the paper.

3. RVE models and finite element simulations

The first step of numerical homogenization is to generate a set of appropriate RVE models which can statistically represent the composite. In the paper, the IPRNC is geometrically simulated by three-dimensional representative cubic unit cell with 27 non-overlapping identical spheres randomly distributed. Because the PBC will be applied to the RVE models in the FEM simulations, it is required that the RVE models have periodic microstructures. That is, if a particle intersects the RVE surface, it has to be split into an appropriate number of parts and copied to the opposite sides of the cube (Fig. 1). Therefore the RVE model can be used as a unit block to build composite models with correct periodic microstructures. The software DIGIMAT 4.1

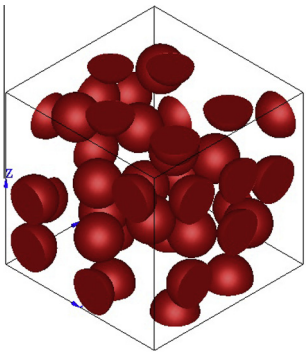

Fig. 1. The microstructure of a RVE model with 20 vol% of particles.

is used to generate RVE models with periodic microstructures. To investigate the effect of different particle volume fraction c, RVE models with various volume fractions (i.e., $c = 5\%$, 10%, 20% and 30%) of particles are generated. For each volume fraction, 4 different RVE samples are created to study the variation of the predictions (an RVE sample with 20 vol% of particles is shown in Fig. 1). The diameter of the particles d in each RVE can be determined by the particle volume fraction c. For example, when $c = 0.3$, $d = 0.2768$ (the size of the RVE cubic unit $L = 1$ here). To prevent severely distorted finite elements in the matrix necking zone between particles, it is required that the distance between any two spheres is larger than $0.1d$ for $c \leqslant 0.2$ and $0.05d$ for $c > 0.2$.

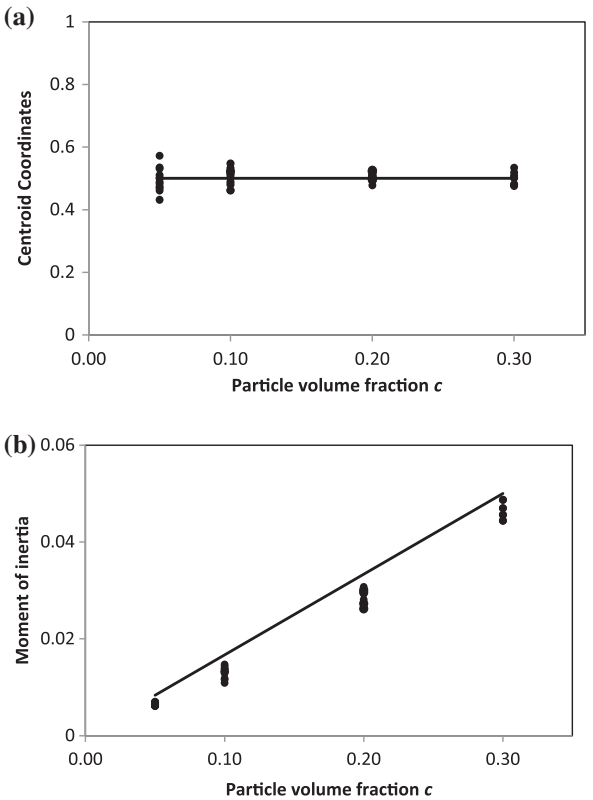

Fig. 2. (a) Coordinates of the centroid of the spherical particles vs. the particle volume fraction c. For each value of c, there are four RVE samples, which produce 12 coordinate values (x, y, z coordinate values for every RVE sample). (b) Moment of inertia, I, of the spherical particles vs. the particle volume fraction c. $I = cL^2/6$ for ideally randomly distributed particles is also plotted in solid line for comparison. Similarly, there are 12 values of I for each value of c (there are I_x, I_y, I_z for every RVE sample).

To correctly predict the mechanical response of the macroscopically isotropic IPRNC, it is important to make sure that the generated RVE models are close to isotropic. The isotropy of the particle distribution in the 16 RVE models is analyzed by computing the positions of the centroid of the particles and their moment of inertia in relation to the three axes which are parallel to the three axes of the coordinate system and pass through the centre of the RVE unit. The results are plotted in Fig. 2. When the particles are ideally random distributed, the moment of inertia is $I = cL^2/6$ (Segurado and Llorca, 2002). This is also plotted in Fig. 2 for comparison. The results in Fig. 2 show that, for all RVE samples, the centroid is always close to $L/2$, and the value of the moment of inertia is also close to the ideal value $cL^2/6$ (the moment of inertia of the particles in an RVE model is usually slightly smaller than the ideal value because the partition of the particles leads to smaller contributions of the particles to the overall moment of inertia). This implies that there are no axial preferential directions identified in the 16 RVE samples. An alternative method to verify the isotropy of an RVE model is to simulate the response of the RVE model under uniaxial tension/compression along various directions, which will be discussed in the next section.

For a given average deformation gradient $\bar{\mathbf{F}}$, based on (5), it is obvious that the choice of boundary condition is not unique. Usually three types of boundary condition are used for general RVE models: (i) the prescribed displacement boundary condition (PDBC); (ii) the prescribed traction boundary condition (PTBC) (or sometimes named as "mixed boundary condition (MBC)"); and (iii) the periodic boundary condition (PBC) (Chen et al., 1999). Chen et al. (1999) investigated the effects of these three types of boundary condition on predictions of RVE models and their results showed that the PBC provides the best performance, while the PDBC and the MBC over and underestimate the yield strength respectively. This observation has been verified by many other researchers (e.g., Hohe and Becker, 2003). Because of this, the PBC is applied to all FEM simulations of the RVE models in the paper. For any given average deformation gradient $\bar{\mathbf{F}}$ applied to the RVE model, the PBC can be represented as the following general format (Guo et al., 2007):

$$\begin{aligned} &\mathbf{x}(Q_1) - \mathbf{x}(Q_2) = \bar{\mathbf{F}}[\mathbf{X}(\mathbf{Q_1}) - \mathbf{X}(\mathbf{Q_2})], \\ &\mathbf{V}(\mathbf{Q_1}) = -\mathbf{V}(\mathbf{Q_2}), \end{aligned} \tag{9}$$

where Q_1 represents a general node on a face of the RVE cube and the corresponding node Q_2 is at the same location of the opposite face of the RVE model. $\mathbf{V}$ is the force applied at the nodes. Here again $\mathbf{X}$ and $\mathbf{x}$ denote the position of a material point respectively in the original (undeformed) and deformed configuration. The first equation in (9) represents the periodic displacements, while the second one represents the antiperiodic traction conditions.

The PBC is implemented by "Equation" type of constraints in ABAQUS 6.10 (ABAQUS, 2010). To implement the PBC, it is essential to have periodic meshes (i.e., identical meshes on each pair of faces of the RVE cube) for the RVE models. The same procedure proposed by Segurado and Llorca (2002) is employed here to mesh the RVE models to guarantee that all the meshes are periodic.

The FEM simulations of all RVE models are performed with ABAQUS/Standard 6.10 within the framework of finite deformation (ABAQUS, 2010). The matrix is modeled as an incompressible neo-Hookean material with $\mu_m = 1$. The particles are also modeled as an incompressible neo-Hookean material and different particle/matrix stiffness ratios are considered, i.e., $\mu_r = 100$, 10, 0.5 ($\mu_r = 0.5$ implies a softer particle inclusion), and the case of rigid particle (which corresponds to $\mu_r = \infty$) is also investigated. In a standard mesh of an RVE model, there are about 60,000 elements for the matrix phase and about 20,000 elements for the particles. Quadratic tetrahedral elements (element type C3D10MH in ABAQUS) are used and around 120,000 nodes are defined. Because of the material and geometric nonlinearity, as well as the severe meshing distortion in the matrix necking zone between spherical particles, convergence is usually very challenging in the numerical simulations (particularly when the stiffness contrast between the particles and the matrix is large) and a typical simulation on an RVE with the standard mesh takes about 4–7 days on an HP Z600 workstation with 16 GB of RAM and 12 CPU cores. To check if this standard mesh is good enough or not to predict accurately the response of the RVE models, an RVE model with $c = 0.2$ is meshed with a refined mesh containing more than 170,000 elements and 200,000 nodes. The uniaxial tension along the X_1 axial direction is simulated for the RVE model with standard and refined meshes respectively. The nominal stress vs. nominal strain (defined as $\varepsilon = \lambda - 1$, where λ denotes the stretch ratio) curves for both meshes are plotted in Fig. 3. The two curves are practically superposed, which implies that the standard mesh is able to predict the mechanical response of the RVE model at almost the same level of accuracy as the refined mesh. Hence the standard mesh is used in all the numerical simulations in the paper due to the limitation of the computing resources. As pointed out in the previous section, any general deformation can be represented by a biaxial deformation provided the model is "overall" isotropic. Therefore the following four types of finite deformations are simulated in the paper: uniaxial tension, uniaxial compression (along the coordinate axial directions and random directions), simple shear and biaxial deformation. For most FEM simulations in the paper, the deformation is applied until convergence is not achieved in ABAQUS with minimum strain increment setting as 0.001. Because of the convergence issue of the proposed numerical approach, all our discussion, if not explicitly expressed, is limited up to the deformation the FEM software can simulate.

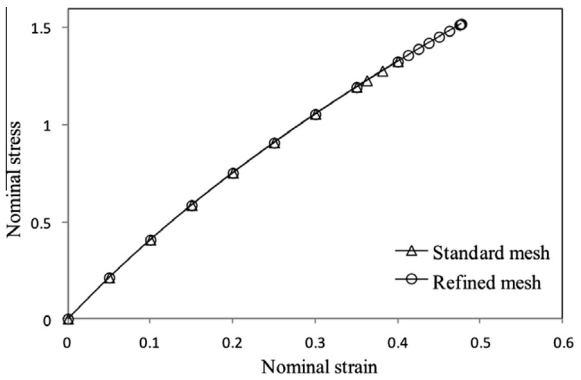

Fig. 3. Results of the FEM simulations of an RVE model ($c = 0.2$, $\mu_r = 10$) subjected to uniaxial tension along the X_1 axial direction with standard (denoted by triangles) and refined meshes (denoted by circles). The curves show the nominal stress and the nominal strain $\varepsilon = \lambda - 1$.

4. Results and discussion

4.1. Size of the RVE in finite deformation

Based on the homogenization theory, an RVE model should be sufficiently large to be statistically representative of the composite (Drugan and Willis, 1996). But because of the limitation of computing resources, practically the size of an RVE model should be chosen such that the RVE model can predict the overall response of the composite with desired accuracy (Drugan and Willis, 1996). Drugan and Willis (1996) showed that within the framework of linear elasticity a small size RVE model can well represent the macroscopic behavior of many composites with reinforcement: for example, the minimum RVE size required to obtain "overall" modulus of the composite with less than 5% error is just about twice of the reinforcement diameter. This is verified by the numerical simulations of the RVE models for the linear elastic PRC (Segurado and Llorca, 2002). For composites with nonlinear phase(s), although there is no theoretical estimates for the minimum RVE size, various numerical investigations showed that similar sizes of RVE models can be used to obtain predictions with the same degree of accuracy (Segurado and Llorca, 2005, 2006).

For hyperelastic composites, however, as pointed out by Moraleda et al. (2009), there is no critical size of the RVE because of the instabilities arising from the non-convexity of the local strain energy functions (Miehe et al., 2002). The numerical simulations of fiber-reinforced composites in finite deformation (Khisaeva and Ostoja-Starzewski, 2006; Moraleda et al., 2009) suggested $L/d \geqslant 16$. However, in our RVE models, $L/d = 3.61$ (for $c = 0.3$) to 6.56 (for $c = 0.05$). If the ratio L/d was increased to 16, more than 390 spheres would be required in the RVE and obviously the corresponding computing cost would be beyond the practical limit. On the other hand, as will be illustrated in this section later, our simulation results show that the variations between the predictions of various RVE models are well below 5% in general, which implies that the small size RVE used in the paper is able to obtain exact responses (to a few percent) of the IPRNC under general three-dimensional finite deformation. That is, similar accuracy can also be obtained for the IPRNC in the finite deformation regime

with small size RVE models comparing to the results in the infinitesimal deformation regime. We note that material instability is not considered in this paper.

4.2. Isotropy of the RVE models

After the random distribution of the particles in the 16 RVE models is verified in the previous section, the isotropy of the mechanical behavior of the RVE models is double-checked by direct simulations of the responses of the RVE models subjected to uniaxial tension/compression along various directions. For an RVE model with $c = 0.2$, $\mu_r = 10$, the nominal stress vs. nominal strain curves for uniaxial tension along the three coordinate axial directions are plotted in Fig. 4. For the three uniaxial tension simulations, convergence problem occurs when the stretch ratio λ reaches about 1.5–1.7. The ultimate stretch ratio obtained by ABAQUS depends on the particle/matrix stiffness ratio, the RVE geometry, the mesh, as well as the stretch direction. The response of the same RVE model subjected to uniaxial tension along a random direction represented by the unit vector $(-0.6461, -0.1411, 0.7501)$ is also simulated and plotted in Fig. 4 (all random directions and numbers used in the paper are generated in MATLAB prior to the ABAQUS simulation). The four curves are practically superposed (relative difference less than 0.85%, which is within the error of the FEM simulation itself). The nominal strains in the two transverse directions are also examined for the four simulations against the isotropic solution $\varepsilon_2 = \varepsilon_3 = \lambda^{-1/2} - 1 = (1 + \varepsilon_1)^{-1/2} - 1$ (Fig. 4). The eight curves from numerical simulation results are very close to the theoretical solution (maximum relative variation less than 1.5%). This indicates that the uniaxial tensile behavior of this RVE model (in the undeformed configuration) is very close to isotropic. Similarly, the FEM simulation results of this RVE model subjected to uniaxial compression along the three coordinate axial directions and a random direction $(0.6366, 0.6433, 0.4253)$ are plotted in Fig. 5. Uniaxial compression can be simulated until about $\lambda = 0.55$. It is clear that the uniaxial compression behavior of this RVE model is also very close to isotropic because the maximum variation between the four simulations is well below 0.9%.

Since both Castaneda (1989) and Bergstrom and Boyce (1999) proposed the use of an incompressible neo-Hookean model to estimate the response of an IPRNC, the strain energy results $\overline{W}$ computed from the FEM simulations of

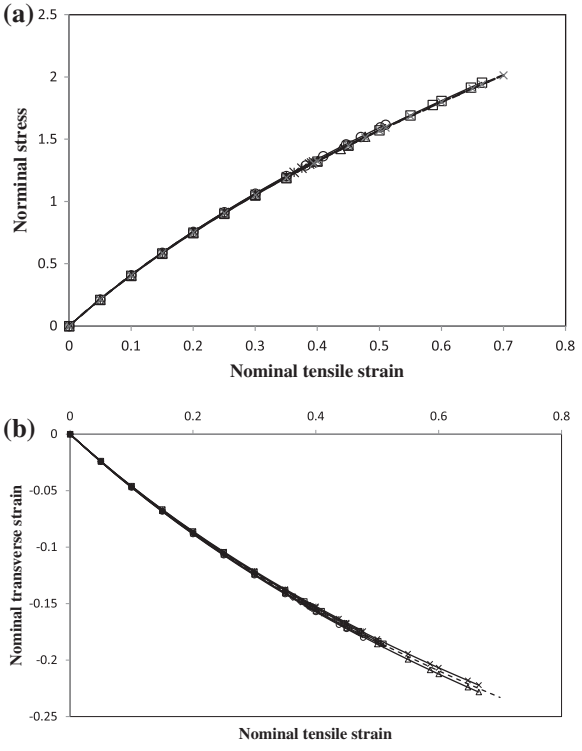

Fig. 4. (a) Nominal stress vs. nominal strain curves of an RVE model ($c = 0.2$, $\mu_r = 10$) subjected to uniaxial tensions along the three axial directions and a random direction $(-0.6461, -0.1411, 0.7501)$. The theoretical nominal stress vs. nominal strain curve from the fitted strain energy function is plotted as a dotted line. (b) The corresponding nominal strains in the transverse directions are also plotted against the nominal tensile strain. The isotropic solution $\varepsilon_2 = \varepsilon_3 = \lambda^{-1/2} - 1 = (1 + \varepsilon_1)^{-1/2} - 1$ is plotted as a dotted line.

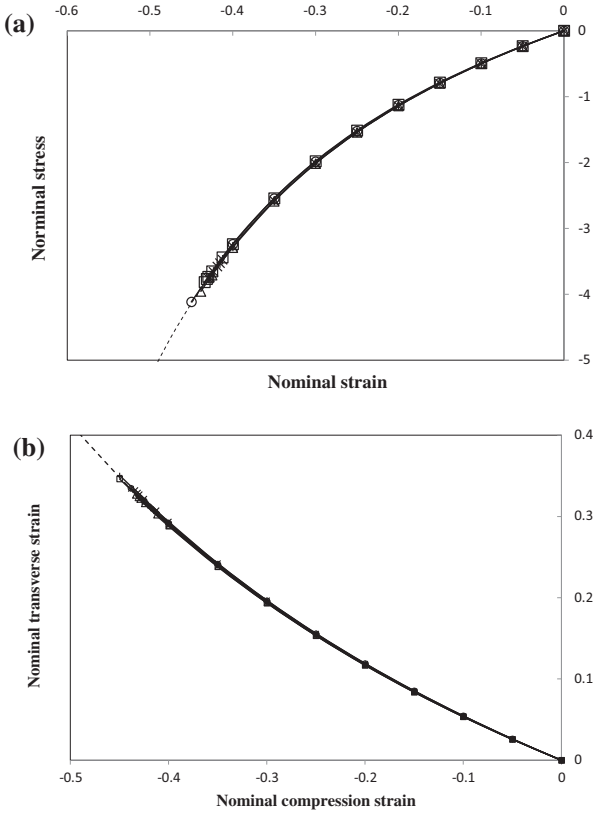

Fig. 5. (a) Nominal stress vs. nominal strain curves of an RVE model ($c = 0.2$, $\mu_r = 10$) subjected to uniaxial compressions along the three axial directions and a random direction $(0.6366, 0.6433, 0.4253)$. The theoretical nominal stress vs. nominal strain curve from the fitted strain energy function is plotted in dotted line. (b) The corresponding nominal strains in the transverse directions are also plotted against the nominal compression strain. The isotropic solution $\varepsilon_2 = \varepsilon_3 = \lambda^{-1/2} - 1 = (1 + \varepsilon_1)^{-1/2} - 1$ is plotted as a dotted line.

the uniaxial tension are plotted against $I_1 - 3$ in Fig. 6. A clear propositional relation is observed and the data is well fitted by $\overline{W} = 0.7441(I_1 - 3)$ using MS Excel 2007 (the coefficient of determination $R^2 = 0.9999$ indicates an excellent fit), which implies the effective shear modulus of the IPRNC is $\mu_c = 1.4882$ for the loading case of uniaxial tension. The theoretical nominal stress–strain curve computed from the fitted strain energy function is plotted as a dotted line in Fig. 4, which is practically identical to the numerical results. The strain energy results $\overline{W}$ computed from the four uniaxial compression simulations are also fitted as $\overline{W} = 0.7459(I_1 - 3)$ in Fig. 6 ($R^2 = 0.9998$ in MS Excel 2007). The corresponding theoretical nominal stress–strain curve obtained from this fitted strain energy function is plotted in dotted line in Fig. 5, which is again practically superposed with the numerical results. The difference between the effective shear moduli of the IPRNC predicted by uniaxial tension and uniaxial compression is less than 0.24%, which suggests that, up to the deformation the FEM software can simulate, a unique incompressible neo-Hookean model might be capable of predicting the mechanical behavior of the IPRNC under general finite

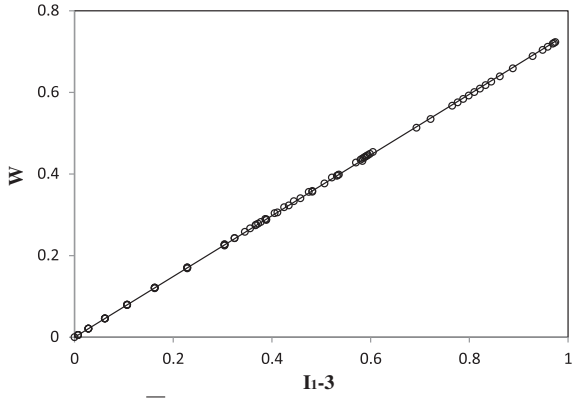

(a) $\overline{W}$ vs. $I_1 - 3$ for uniaxial tension simulations

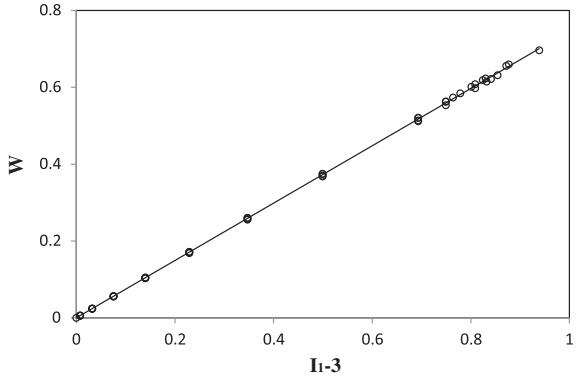

(b) $\overline{W}$ vs. $I_1 - 3$ for uniaxial compression simulations

Fig. 6. (a) The strain energy results $\overline{W}$ computed from four FEM simulations of an RVE model ($c = 0.2$, $\mu_r = 10$) subjected to uniaxial tensions are plotted against $I_1 - 3$. The data is fitted by $\overline{W} = 0.7441(I_1 - 3)$ (solid line). (b) The strain energy results $\overline{W}$ computed from four FEM simulations of an RVE model ($c = 0.2$, $\mu_r = 10$) subjected to uniaxial compressions are plotted against $I_1 - 3$. The data is fitted by $\overline{W} = 0.7459(I_1 - 3)$ (solid line).

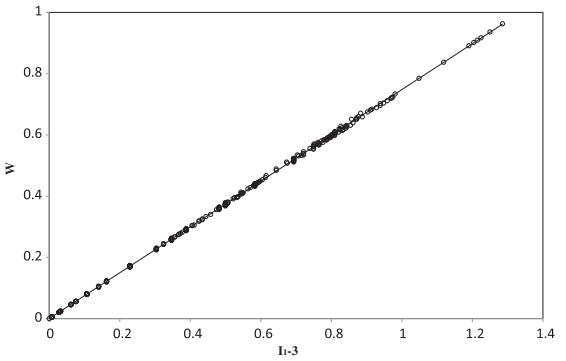

Fig. 7. Average strain energy $\overline{W}$ vs. $I_1 - 3$ for the 20 uniaxial tension/compression simulations of 4 RVE models ($c = 0.2$, $\mu_r = 10$). The linear fitting curve is plotted in solid line.

deformation. Similar procedure is applied to all 16 RVE models to examine their isotropy. The simulation results show that, for any RVE model, its responses under uniaxial tension or compression along different directions can all be well described by a unique incompressible neo-Hookean model. The differences between the effective shear moduli predicted by various tension or compression simulation cases for one RVE model is well below 4.6%. Therefore the isotropy of the 16 RVE models is confirmed directly by the FEM simulations.

To study the variations between different RVE models, the other three RVE models with $c = 0.2$ are subjected to uniaxial tension along the X_1 and X_2 axial directions, as well as uniaxial compression along the X_3 axial directions and a random direction in FEM simulations ($\mu_r = 10$). In Fig. 7, all the computed strain energy data $\overline{W}$ from the 20 simulations is plotted against $I_1 - 3$ and they are fitted excellently by a linear relation $\overline{W} = 0.7479(I_1 - 3)$ in MS Excel 2007 ($R^2 = 0.9999$). The effective shear moduli of the 4 RVE model are obtained individually (by fitting the corresponding simulation results on each RVE model) as $\mu_c = 1.4896$, 1.4948, 1.505, 1.5064, respectively. The relative differences between these effective shear moduli are less than 1.2%. This shows again that the small size RVE models used here are able to obtain exact responses (to a few percent) of the IPRNC.

4.3. Composites embedded with rigid particles

When the particles are rigid (i.e., $\mu_r = \infty$), each particle component (some particles are partitioned into several components by the RVE surface) is defined as a rigid body using the nodes on its matrix-particle surface. Hence there is no need to discretize it into elements (Fig. 8). If a spherical particle is divided into several components by the RVE surface, the translational and rotational degrees of freedom (d.o.f.s) of those components are constrained properly to make sure the PBC is satisfied on the RVE surface. This can be verified, for example, by the deformed shape of an RVE model with 5 vol% rigid particles under uniaxial tension (Fig. 8).

Three simple deformations, i.e., uniaxial tension (along the X_1 axial direction and up to $\lambda_1 = 1.85$), uniaxial compression (along the X_3 axial direction and up to

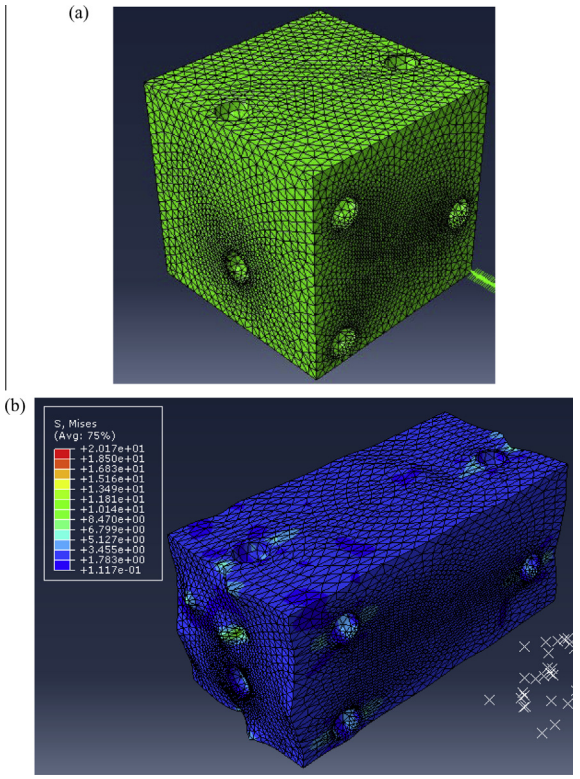

Fig. 8. An RVE model with 5 vol% of rigid particles (a) and its deformed shape after uniaxial tension (b).

$\lambda_3 = 0.60$) and simple shear (in the X_1X_2 plane and up to $k = 0.32$), are simulated for an RVE model with $c = 0.05$. The nominal stress–strain curves are plotted in Fig. 9. Numerical simulation of a biaxial deformation with nominal strain ratio $\varepsilon_2/\varepsilon_1$ randomly assigned as -0.3432 (because only $\lambda_1 \geqslant \lambda_2 \geqslant \lambda_1^{-1/2}$ needs to be considered, a random value between -0.5 and 1 is assigned to $\varepsilon_2/\varepsilon_1 = (\lambda_2 - 1)/(\lambda_1 - 1)$) is performed (up to $\varepsilon_1 = 0.85$) to check the response of the RVE model under general three-dimensional finite deformation. The nominal stress–strain (in the X_1 direction only) curve is plotted in Fig. 9. The strain energy $\overline{W}$ obtained from the four simulations is plotted against $I_1 - 3$ in Fig. 10 and they are fitted excellently by a linear relation $\overline{W} = 0.5687(I_1 - 3)$ in MS Excel 2007 ($R^2 = 1.0$, and relative error (between the fitted function and the numerical data) well below 0.23%). Therefore the effective shear modulus of the RVE model is predicted as $\mu_c = 1.1374$. The theoretical nominal stress–strain curves from the effective shear modulus are plotted as dotted lines in Fig. 9, which are almost identical to the numerical results (maximum relative error less than 1.6%).

FEM simulations on other three RVE models with $c = 0.05$ are required to obtain an "average" effective shear modulus of the IPRNC with $(c = 0.05, \mu_r = \infty)$. Ideally all the four types of deformations should be examined on every RVE model to compute the effective shear modulus, however, because of the extensive computing time required for the simulations, the following timesaving strategy is used: to compute the effective shear modulus for a given (c, μ_r) case, the following three requirements are satisfied: (i) at least 6 FEM simulations are performed; (ii) all four types of deformations are simulated; and (iii) all four related RVE models (with the particular volume ratio) are involved. Then the strain energy data from all the FEM simulations are collected together to fit the effective shear modulus of the IPRNC. For example, eight FEM simulations are performed on the 4 RVE models for the IPRNC with $(c = 0.05, \mu_r = \infty)$ discussed above, and the effective shear modulus is computed by fitting all the strain energy data from the eight simulations as $\mu_c = 1.1376$. To investigate the variation between the effective shear moduli of different FEM simulations, the effective shear modulus of every simulation is calculated by fitting related strain energy data and the maximum and minimum effective shear moduli are recorded to compare with the average effective shear modulus. For the IPRNC with $(c = 0.05, \mu_r = \infty)$, the maximum and minimum values of the eight computed effective shear moduli are $\mu^c_{\max} = 1.1404$ and $\mu^c_{\min} = 1.1350$, and they are represented by the error bars in Fig. 11.

Similarly, the effective shear modulus of the IPRNC can be computed numerically for $c = 0.1, 0.2, 0.3$ (we note that for RVE models with large rigid particle volume fraction value, ABAQUS standard can only simulate a relatively limited extent of deformation because all deformations are carried by the matrix phase and the mesh in the matrix necking zones between close particles is severely distorted at even the early state of the deformation). The obtained moduli are plotted in Fig. 11 as a function of the particle volume fraction.

Based on the concept of strain amplification, Bergstrom and Boyce (1999) assumed that the composite is still a neo-Hookean material and they proposed the following estimate of shear modulus for incompressible neo-Hookean composite embedded with rigid particles:

$$\mu_c = \mu_m(1 - c)(1 + 3.5c + 30c^2). \tag{10}$$

Castaneda (1989) also assumed the neo-Hookean behavior of the composite and gave a self-consistent estimate of the effective shear modulus of the IPRNC as follows:

$$\mu_c = \frac{\sqrt{[(1-3c)\mu_r + (3c-2)\mu_m]^2 + 8\mu_m\mu_r} - [(1-3c)\mu_r + (3c-2)\mu_m]}{4}. \tag{11}$$

When the particles are rigid, it leads to the following result (Castaneda, 1989)

$$\mu_c = \frac{\mu_m}{1 - 3c}. \tag{12}$$

Obviously it will overestimate μ_c when $c \to 1/3$. The strain amplification estimate, SAE (Bergstrom and Boyce, 1999), and the self-consistent estimate, SCE (Castaneda, 1989) are both plotted in Fig. 11 to be compared with the numerical results. Because the dispersion of the values of the effective shear moduli obtained from different RVE models (maximum and minimum values illustrated by the error bars in Fig. 11) is remarkably small in all cases (less than 2.1%), the numerical results can be taken as a very close approximation to the "exact" solution. From Fig. 11, it can be found that both the SCE and the SAE over-

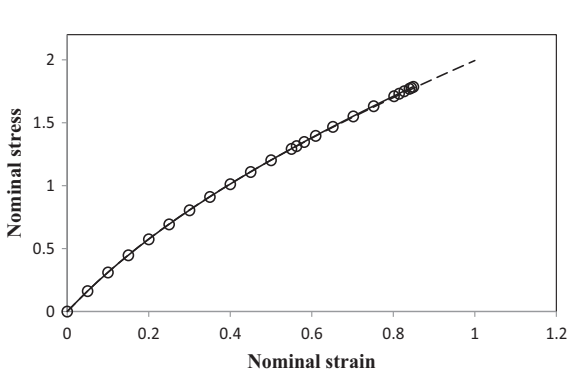

(a) Nominal stress P_{11} vs. nominal strain ε_1 for uniaxial tension simulation

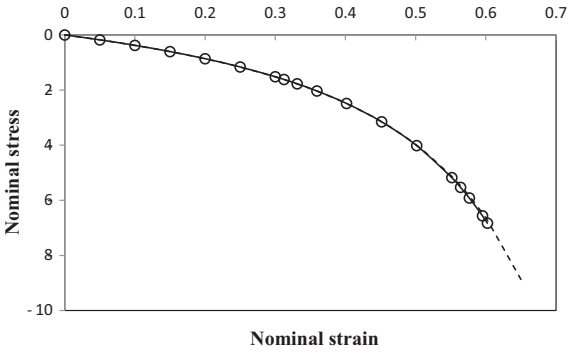

(b) Nominal stress P_{33} vs. nominal strain ε_3 for uniaxial compression simulation

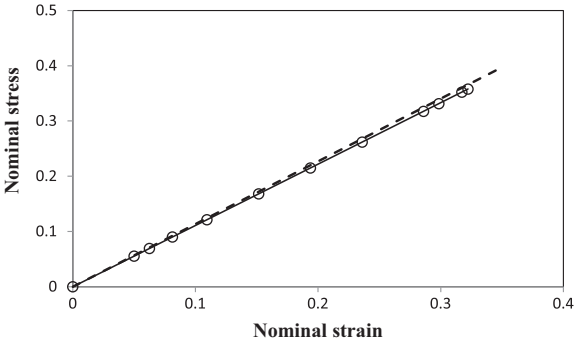

(c) Nominal shear stress P_{12} vs. nominal shear strain F_{12} for simple shear simulation

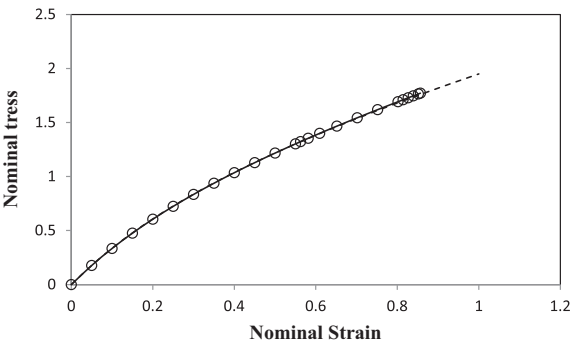

(d) Nominal stress P_{11} vs. nominal strain ε_1 for simulation of a biaxial deformation

Fig. 9. Simulation results of an RVE model with 5 vol% of rigid particles: (a) nominal stress P_{11} vs. nominal strain ε_1 for uniaxial tension simulation along the X_1 axial direction (up to $\lambda_1 = 1.85$); (b) nominal stress P_{33} vs. nominal strain ε_3 for uniaxial compression simulation along the X_3 axial direction (up to $\lambda_3 = 0.6$); (c) nominal shear stress P_{12} vs. nominal shear strain F_{12} for simple shear simulation in the X_1X_2 plane (up to $k = F_{12} = 0.32$); (d) nominal stress P_{11} vs. nominal strain ε_1 for simulation of a biaxial deformation with nominal strain ratio $\varepsilon_1/\varepsilon_2 = -0.3424$. The theoretical nominal stress–strain curve from the effective shear modulus is plotted as a dotted line in each figure.

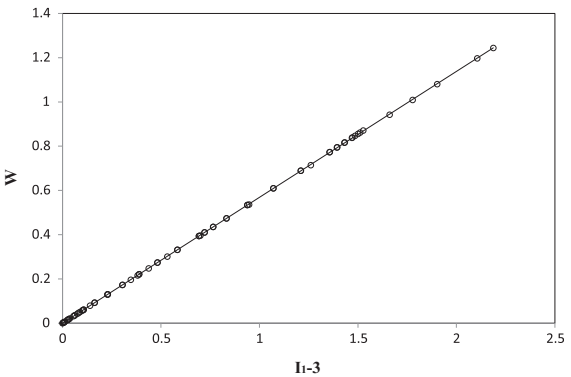

Fig. 10. Average strain energy $\overline{W}$ vs. $I_1 - 3$ for four numerical simulations of an RVE model with 5 vol% of rigid particles. The linear fitting curve is plotted as a solid line.

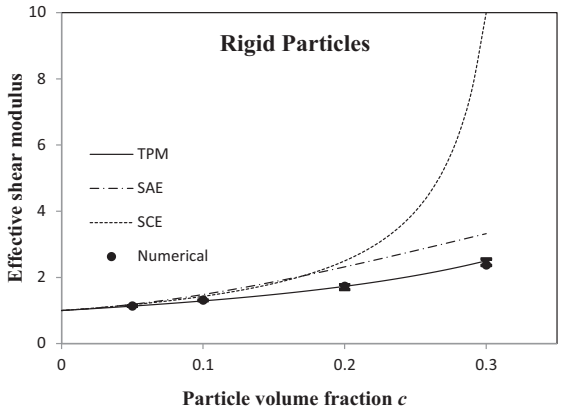

Fig. 11. The effective shear moduli computed from numerical homogenization for IPRNC with rigid particles are compared with the SAE, SCE, and TPM predictions.

estimate μ_c when $c > 0.1$. When $c = 0.05$, the prediction of the SCE and the SAE are about 3.42% and 4.39% larger than the numerical result, respectively. The errors increase up to 8.47% and 12.8% when $c = 0.1$. For moderate particle volume fraction $c = 0.2$, 44.3% and 33.9% errors are introduced to the SCE and the SAE predictions, respectively. The SCE result is actually not useable when $c > 0.2$: it will overestimate three times the value of μ_c when $c = 0.3$. The SAE prediction overestimate μ_c by 39.8% when $c = 0.3$.

Because the large deformation estimates for PRC cannot well predict the effective modulus of the IPRNC with rigid particles, the classical results for PRC in infinitesimal deformation regime are examined. Since the formula proposed by Christensen and Lo (1979) based on the three phase model (TPM) for the effective shear modulus of the linear elastic PRC agrees very well with the numerical homogenization results under small strain (Segurado and Llorca, 2002) and is relatively simple, it is chosen to be compared with our numerical results under large deformation (Fig. 11). Surprisingly, the TPM model originally developed for linear elastic PRC provides a much better prediction than the large deformation formulae. The differences between the predictions of the TPM model and the numerical results are only 0.39%, 2.05%, 0.22%, 5.08% for $c = 0.05$, 0.1, 0.2, and 0.3, respectively.

Recently Avazmohammadi and Castaneda (2012) proposed a TSO model to estimate the strain energy function of the IPRNC with rigid inclusions. In this model the behavior of the composite is no longer assumed as neo-Hookean type. Although the explicit formula of the strain energy function for general deformation status is rather lengthy (which reflect the complex nature of the problem), the expression can be significantly simplified for special cases such as uniaxial tension, simple shear, equi-biaxial tension (which is equivalent to uniaxial compression). The stress results from the numerical simulations of the uniaxial tension (UT), simple plane shear (PS), and uniaxial compression (UC, which is equivalent to the equi-biaxial tension, ET) loading cases are plotted in Fig. 12 and compared with the TSO model. When the volume fraction of the particles c is small (i.e., $c = 5\%$, 10%), the curves predicted by the TSO model fit the numerical results very well for all cases (relative error less than 3.7%). This implies that the mechanical responses of the composites predicted by the TSO model are very close to the neo-Hookean model within the regime that the numerical simulation can reach. This is further verified by the almost linear W vs. $I_1 - 3$ curves of the TSO model in Fig. 13 for three loading cases. When the volume fraction of the particles increases (i.e., $c = 20\%$, 30%), though the stress and strain energy predicted by the TSO model is slightly smaller than the numerical results (relative errors up to 14%, Figs. 12 and 13c,d), the relations between W vs. $I_1 - 3$ are still very close to linear within the moderate deformation regime. We note that the TSO model will behave differently from neo-Hookean model when the deformation of the IPRNC is significantly large.

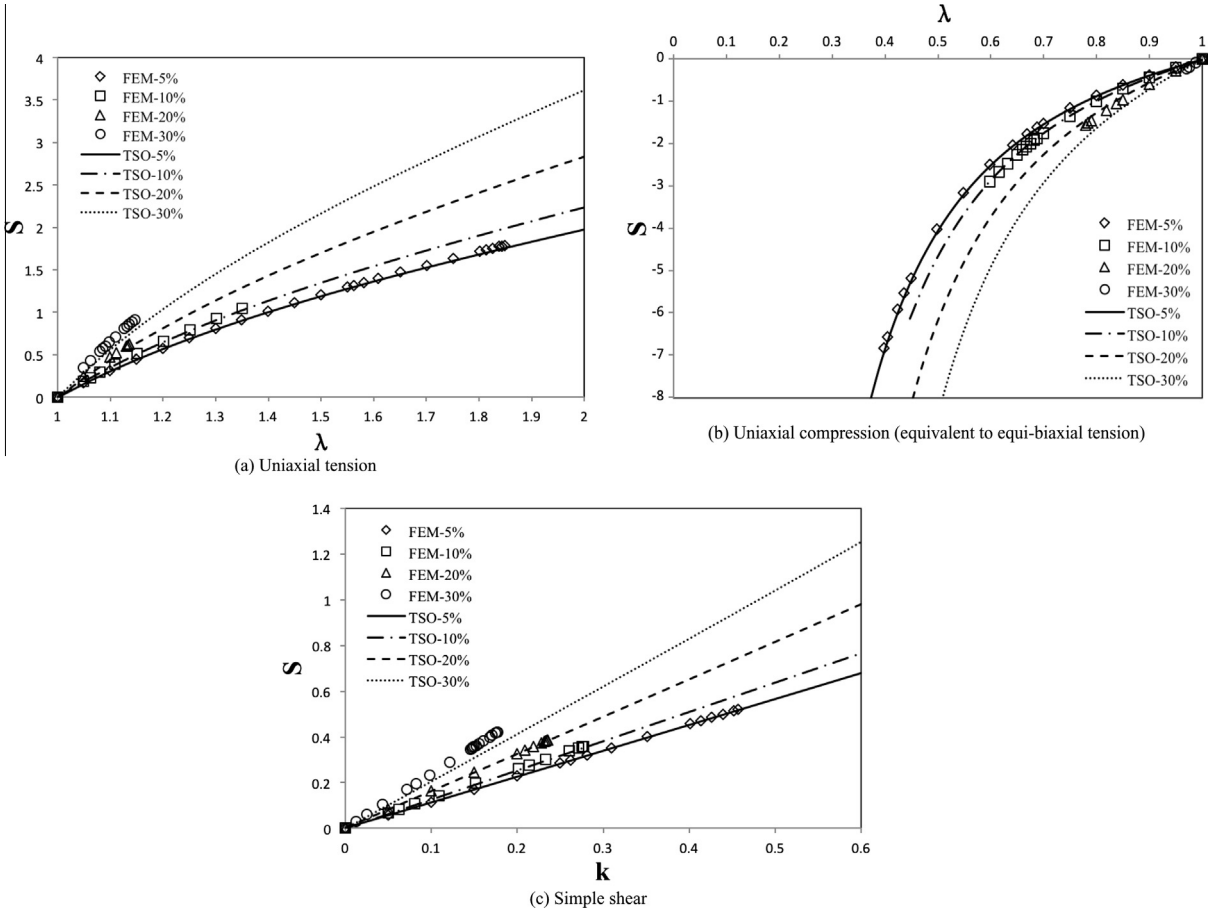

(a) Uniaxial tension

(b) Uniaxial compression (equivalent to equi-biaxial tension)

(c) Simple shear

Fig. 12. The nominal stress–deformation curves predicted by TSO model for (a) uniaxial tension, (b) uniaxial compression (equivalent to equi-biaxial tension), and (c) simple shear simulations respectively. The numerical results are plotted for comparison.

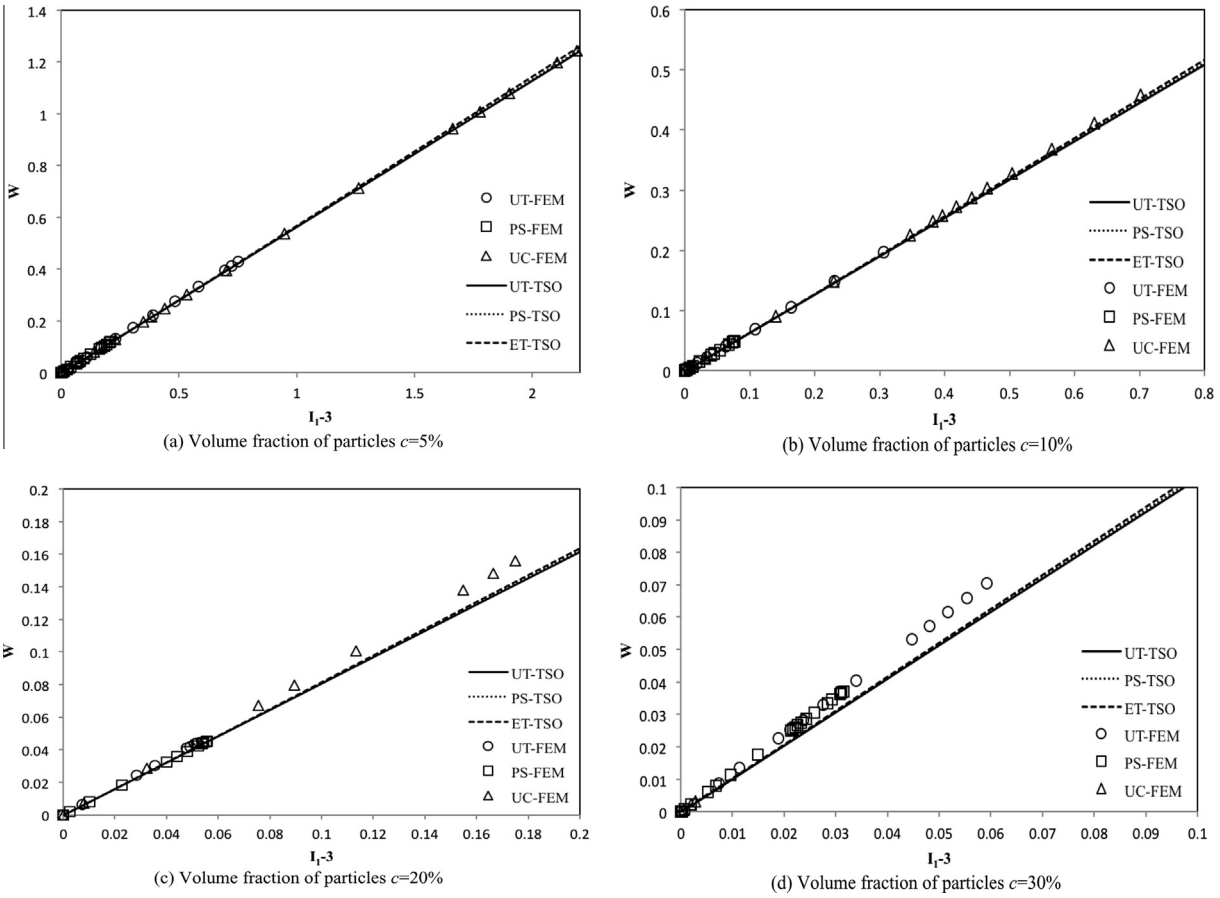

Fig. 13. The strain energy $\overline{W}$ vs. $I_1 - 3$ curves predicted by TSO model for IPRNC with rigid particles. The volume fraction of the particles c = (a) 5%, (b) 10%, (c) 20%, and (d) 30%, respectively. The numerical results are plotted for comparison.

4.4. Particles 100 times stiffer than matrix

FEM simulations are carried out on the IPRNC with large but finite stiffness contrast between particles and matrix ($\mu_r = 100$). Again the effective shear modulus are obtained by simulations of four types of deformations, i.e., uniaxial tension along the X_1 axial direction (up to $\lambda_1 = 1.46$), uniaxial compression along the X_3 axial direction (up to $\lambda_3 = 0.59$), simple shear in the X_1X_2 plane (up to $k = 0.77$), and general biaxial deformation ($\varepsilon_2/\varepsilon_1 = 0.8116$ up to $\varepsilon_1 = 0.24$) on an RVE with $c = 0.1$. The nominal stress–strain curves are shown in Fig. 14(a)–(c) for uniaxial tension, uniaxial compression and simple shear simulations, while the strain energy $\overline{W}$ computed in the four simulations of this RVE is plotted against $I_1 - 3$ in Fig. 14(d). The observed linear relation between $\overline{W}$ and $I_1 - 3$ is fitted by $\bar{W} = 0.6457(I_1 - 3)$ ($R^2 = 1$ in MS Excel 2007). The effective shear moduli computed from numerical homogenization for the IPRNC with $\mu_r = 100$ are compared with the SCE, TPM predictions in Fig. 15. The variations represented by the error bars are all below 4.25% (Fig. 15). The TPM model matches the numerical results very well and the differences for $c = 0.05$, 0.1, 0.2, 0.3 are only 0.41%, 0.96%, 0.22% and 3.82%, respectively. The SCE result will overestimate the shear modulus significantly when $c > 0.1$, and the relative errors are 3.14%, 8.69%, 36.39% and 123.77% for $c = 0.05$, 0.1, 0.2, 0.3, respectively.

4.5. Particles 10 times stiffer than matrix

To explore the case that the particle stiffness is comparable to the matrix stiffness, a set of simulations is performed for $\mu_r = 10$ in ABAQUS. Because previously the uniaxial tension and the uniaxial compression deformations have already been investigated extensively to verify the isotropy of the RVE models, only simple shear and general biaxial simulations are required. To validate the neo-Hookean model for the IPRNC, eight series of biaxial simulations ($\varepsilon_2/\varepsilon_1 = 1$, 0.8, 0.6, 0.4, 0.2, 0, -0.2, -0.4) as well as the simple shear simulation (up to $k = 1.0$) are performed on an RVE model with $c = 0.2$ to cover a significant amount of general deformations. All the $\overline{W}$ vs. $I_1 - 3$ data from 34 FE simulations (9 biaxial, 3 simple shear, 12 uniaxial tension and 10 uniaxial compression simulations) for the IPRNC with ($c = 0.2$, $\mu_r = 10$) is fitted by the linear relation $\bar{W} = 0.7480(I_1 - 3)$ (e.g., $\mu = 1.4960$) in Fig. 16, which is consistent with the effective shear modulus obtained from the uniaxial tension simulations in Section 4.2

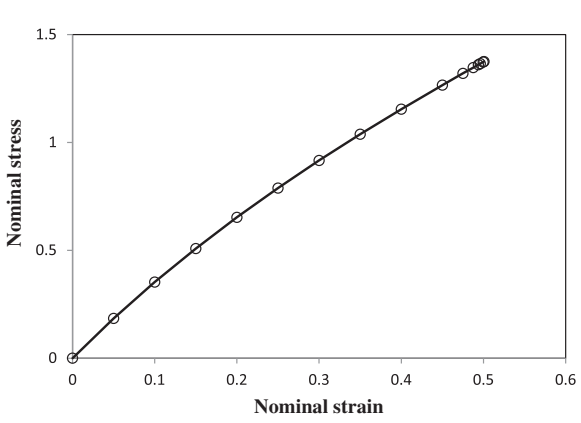

(a) Nominal stress vs. nominal strain for uniaxial tension simulation

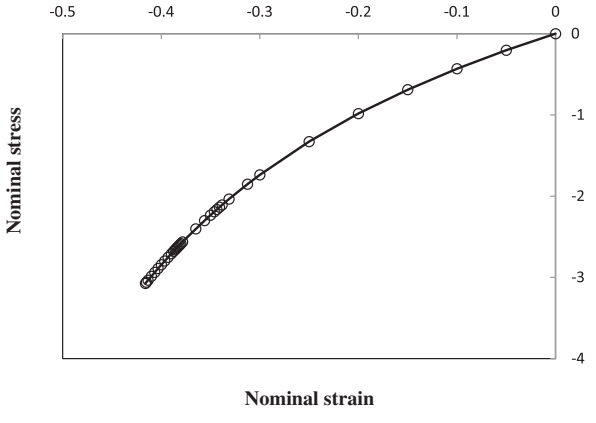

(b) Nominal stress vs. nominal strain for uniaxial compression simulation

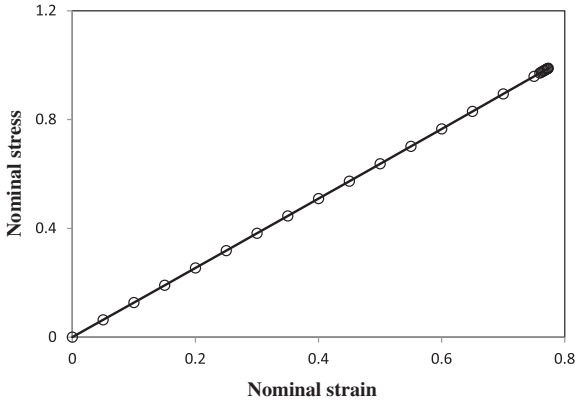

(c) Nominal shear stress vs. nominal shear strain for simple shear simulation

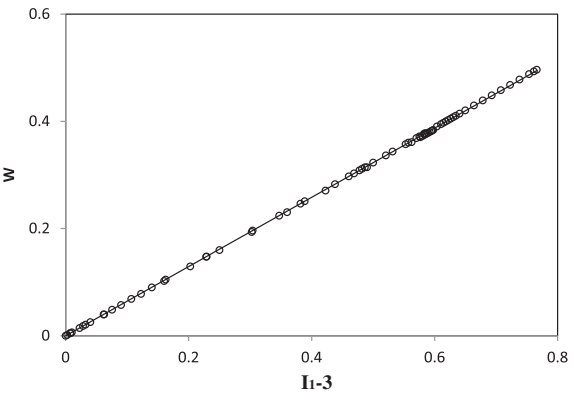

(d) Strain energy $\overline{W}$ vs. $I_1 - 3$

Fig. 14. The nominal stress–strain curves are shown in (a), (b) and (c) for uniaxial tension, uniaxial compression and simple shear simulations respectively, while the obtained strain energy $\overline{W}$ is plotted against $I_1 - 3$ for an RVE ($c = 0.1,\ \mu_r = 100$) in (d).

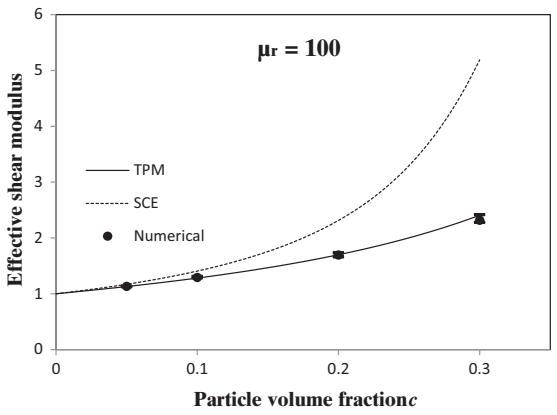

Fig. 15. The effective shear moduli computed from numerical homogenization for IPRNC with $\mu_r = 100$ are compared with the SCE, TPM predictions.

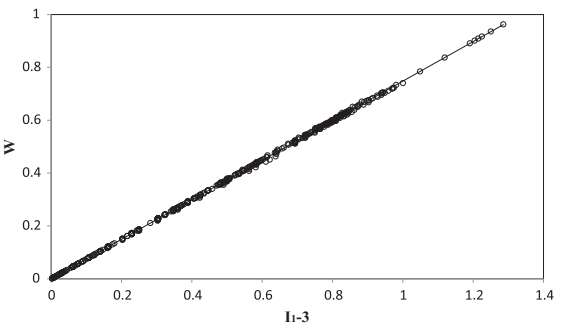

Fig. 16. All the $\overline{W}$ vs. $I_1 - 3$ data from 34 FE simulations (9 biaxial, 3 simple shear, 12 uniaxial tension and 10 uniaxial compression simulations) for the IPRNC ($c = 0.2, \mu_r = 10$) are fitted by the linear relation $\overline{W} = 0.7480(I_1 - 3)$ ($R^2 = 0.9998$).

($\mu = 1.4958$). The maximum and minimum effective shear moduli from individual simulation are $\mu^c_{\max} = 1.5190$ and $\mu^c_{\min} = 1.4526$, which implies the variations of the effective shear moduli are within 4.5%. This clearly indicates that the IPRNC can be well predicted by a neo-Hookean model.

The numerical results for the effective shear modulus are plotted in Fig. 17 together with the predictions of the SCE and TPM models, and the reported dispersions in the

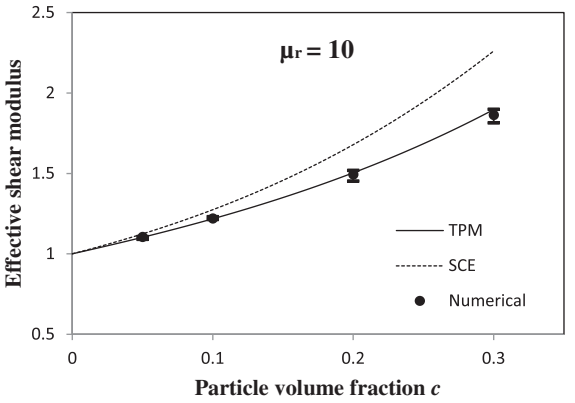

Fig. 17. The effective shear moduli computed from numerical homogenization for IPRNC with $\mu_r = 10$ are compared with the SCE and TPM predictions.

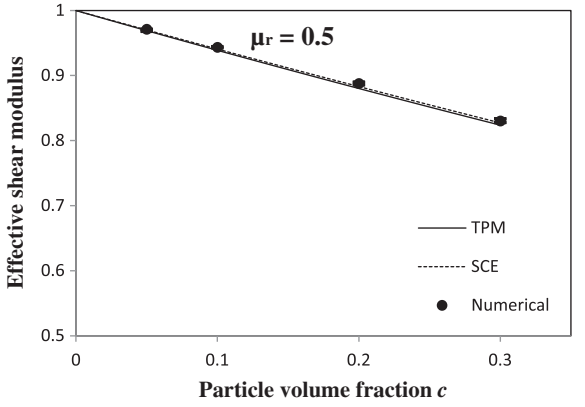

Fig. 19. The effective shear moduli computed from numerical homogenization for IPRNC with $\mu_r = 0.5$ are compared with the SCE and TPM predictions.

numerical simulation are less than 4.56%. Again the TPM model represents an excellent approximation of the numerical results and the maximum difference for $c = 0.3$ is only 1.8%. The SCE model still overestimates the shear modulus by 1.65%, 4.41%, 12.36% and 21.32%, respectively, for $c = 0.05$, 0.1, 0.2, 0.3, though the introduced error for a given volume fraction is smaller than that of the IPRNC with $\mu_r = 100$. This is expected because the

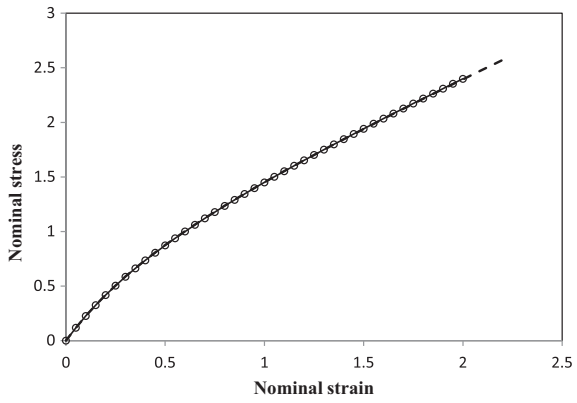

(a) Nominal stress vs. nominal strain for uniaxial tension simulation

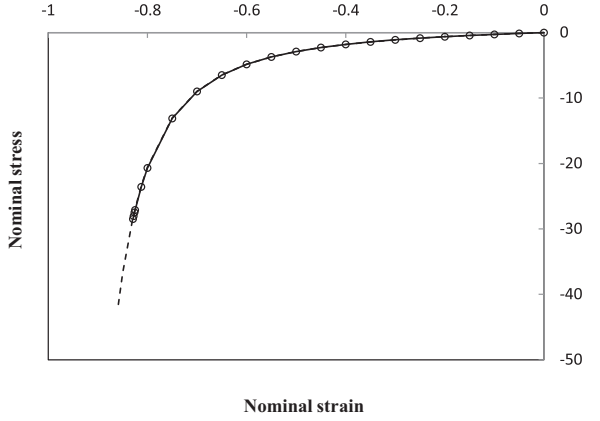

(b) Nominal stress vs. nominal strain for uniaxial compression simulation

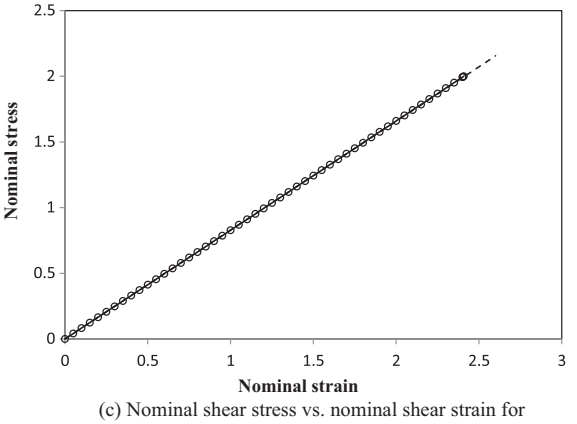

(c) Nominal shear stress vs. nominal shear strain for simple shear simulation

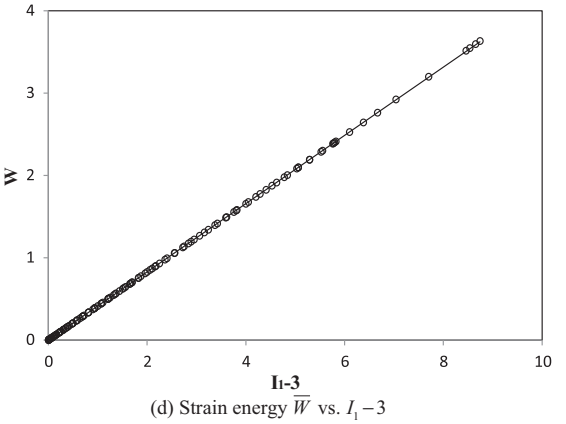

(d) Strain energy $\overline{W}$ vs. $I_1 - 3$

Fig. 18. The nominal stress–strain curves are shown in (a), (b) and (c) for uniaxial tension, uniaxial compression and simple shear simulations respectively, while the obtained strain energy $\overline{W}$ is plotted against $I_1 - 3$ for an RVE ($c = 0.3$, $\mu_r = 0.5$) in (d).

difference between the stiffness of the particles and the matrix is smaller due to the reinforcement of less stiff particles.

4.6. Matrix twice stiffer than particles

In previous simulations, the particles are always stiffer than the matrix. The opposite case (i.e., the matrix is stiffer than the particles) is considered here to fully examine the effect of stiffness contrast between particles and matrix. A small stiffness contrast ($\mu_m/\mu_r = 2$, or $\mu_r = 0.5$) is used to make relatively large deformation possible in the numerical simulation (the convergence problem usually occurs at relatively moderate deformation in previous simulations, which partially comes from the large stiffness contrast, i.e., $\mu_r/\mu_m \geqslant 10$). The FEM simulations of uniaxial tension (up to $\lambda_1 = 2.0$), uniaxial compression (up to $\lambda_3 = 0.17$), simple shear (up to $k = 2.40$), and general biaxial ($\varepsilon_2/\varepsilon_1 = -0.4025$ up to $\varepsilon_1 = 1.0$) deformation are performed on an RVE with $c = 0.3$. The strain energy data $\bar{W}$ from all the 4 simulations are fitted in Fig. 18(d) and the obtained effective shear modulus $\mu_c = 0.8296$. The nominal stress–strain curves are shown in Fig. 18(a)–(c), which are almost identical to the theoretical results based on the computed effective shear modulus. This suggests that the IPRNC's response at significant stretch still follows the neo-Hookean model's prediction.

The effective shear moduli derived from the FEM simulation results are shown in Fig. 19 with maximum dispersions represented by error bars (all less than 0.7%). The numerical results are also compared with the theoretical approximations of the SCE and TPM models. Because the stiffness contrast between the particles and the matrix is small, the effective shear moduli of the IPRNC are close to the shear modulus of the matrix. It is then not surprising that both the SCE and TPM models agree well with the

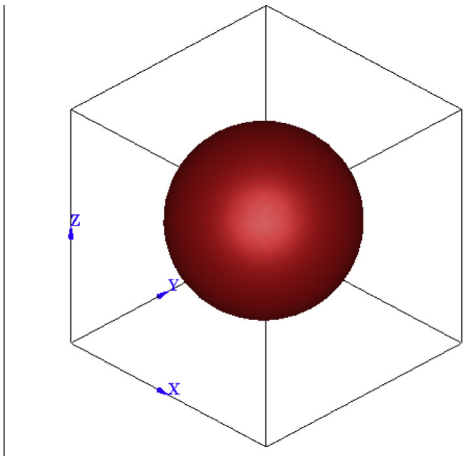

(a) Undeformed

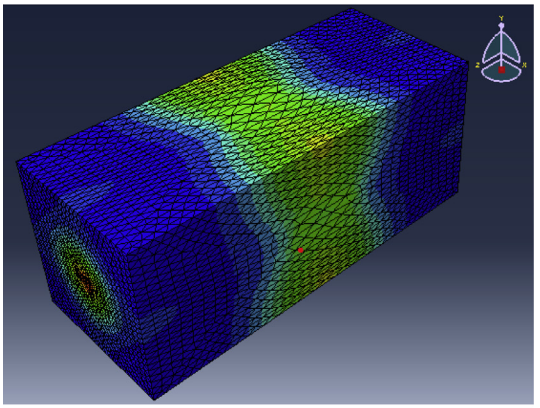

(b) Deformed (100% uniaxial tension)

Fig. 20. Undeformed (a) and deformed (b) simple "one particle in the centre" unit cell model. The shown deformation is 100% uniaxial tension.

Table 1
Deformation range represented by I_1 for all the FE simulations.

c	$\mu r/\mu m$			
	0.5	10	100	∞
0.05	17.55 ($\lambda = 4.13$) 13.71 ($\lambda = 0.14$) 13.68 ($k = 3.26$) 5.03	4.96 ($\lambda = 1.98$) 6.31 ($\lambda = 0.32$) 4 ($k = 1$) * 5.66	3.87 ($\lambda = 1.62$) 3.74 ($\lambda = 0.58$) 4 ($k = 1$) * 3.41	4.5 ($\lambda = 1.84$) 5.19 ($\lambda = 0.39$) 3.21 ($k = 0.45$) 4.53
0.1	17.16 ($\lambda = 4.08$) 17.79 ($\lambda = 0.11$) 10.42 ($k = 2.72$) 8.17	4.4 ($\lambda = 1.81$) 5.02 ($\lambda = 0.41$) 4 ($k = 1$) * 4.49	3.58 ($\lambda = 1.49$) 3.77 ($\lambda = 0.58$) 3.60 ($k = 0.77$) 3.47	3.31 ($\lambda = 1.35$) 3.66 ($\lambda = 0.60$) 3.08 ($k = 0.28$) 3.3
0.2	14.36 ($\lambda = 3.71$) 19.63 ($\lambda = 0.10$) 11.96 ($k = 2.99$) 7.81	4.22 ($\lambda = 1.75$) 4.29 ($\lambda = 0.49$) 4 ($k = 1$) * 3.9	3.35 ($\lambda = 1.37$) 3.41 ($\lambda = 0.67$) 3.6 ($k = 0.77$) 3.43	3.05 ($\lambda = 1.13$) 3.17 ($\lambda = 0.78$) 3.06 ($k = 0.24$) 3.25
0.3	13.77 ($\lambda = 3.63$) 11.74 ($\lambda = 0.17$) 8.80 ($k = 2.40$) 5.06	3.51 ($\lambda = 1.46$) 3.92 ($\lambda = 0.55$) 3.53 ($k = 0.72$) 3.43	3.08 ($\lambda = 1.17$) 3.14 ($\lambda = 0.8$) 3.07 ($k = 0.27$) 3.15	3.06 ($\lambda = 1.14$) 3.003 ($\lambda = 0.96$) 3.03 ($k = 0.17$) 3.006

* The simulations finished without convergence problems.

numerical results. The maximum errors for $c = 0.3$ are only 0.36% and 0.76% for the SCE and TPM models, respectively.

4.7. Deformation ranges of the FE simulations

A total number of 152 FE simulations have been performed on the 16 RVE models. The strain energy $\bar{W}$ computed from each FE simulation shows a clear linear proportional relation with $I_1 - 3$, which suggests a neo-Hookean type response and the corresponding effective shear modulus can be obtained by data fitting for each FEM simulation. The dispersions of fitted effective shear moduli are within 7.5% as shown in Figs. 10, 12, 14 and 16.

It should be noted that convergence is a big issue in our numerical simulations even for RVE models with very refined mesh (e.g., with more than 200,000 elements), particularly when the stiffness contrast between the particles and the matrix is large (e.g., $\mu_r = \infty$, 100). Because we can only claim the neo-Hookean type response of the IPRNC with the deformations simulated by our FEM simulations, it is worthy to report the deformation ranges of the FEM simulations for various IPRNC in Table 1, in which the deformation range is represented by the maximum I_1 reached by the FEM simulations, as well as the principal stretches for uniaxial tension/compression, or nominal shear strain for simple shear deformation. For IPRNCs with particular volume fraction of particles, the larger the stiffness contrast between the particles and the matrix, the smaller deformation range the FE simulations can reach. For IPRNCs with particular μ_r/μ_m, the larger the volume fraction of particles, the more limited the FEM simulations. The reason is that larger volume fraction of particles usually means more severe mesh distortion at the necking area between particles due to the deformation localization. It should be noted that the uniaxial tension, pure shear and equibiaxial tension behaviors of an INRNC with ($c = 0.1,\ \mu_r = \infty$) predicted by Avazmohammadi and Castaneda (2012) (as in Fig. 11 there) are very close to neo-Hookean behavior for $I_1 < 5$.

4.8. One particle unit cell model

The simple "one particle in the centre" unit cell model (Fig. 20) is sometimes used in the literature to simulate PRC (Bergstrom and Boyce, 1999). This type of unit cell represents composites embedded with cubic arrays of spheres (Cohen, 2004), which is macroscopically orthotropic. To examine the mechanical responses of the IPRNC

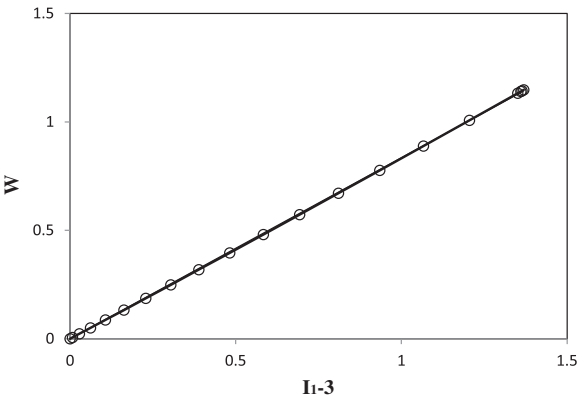

(a) Strain energy $\overline{W}$ vs. $I_1 - 3$ for uniaxial tension simulation

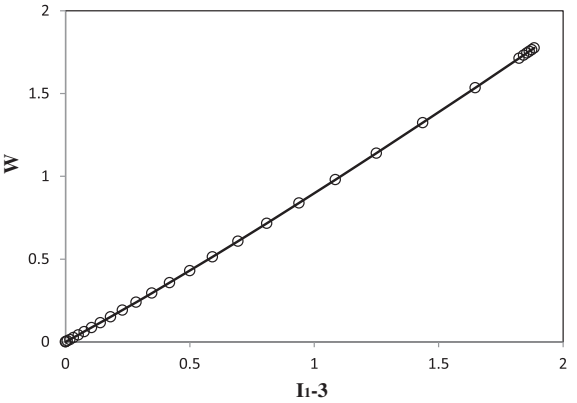

(b) Strain energy $\overline{W}$ vs. $I_1 - 3$ for uniaxial compression simulation

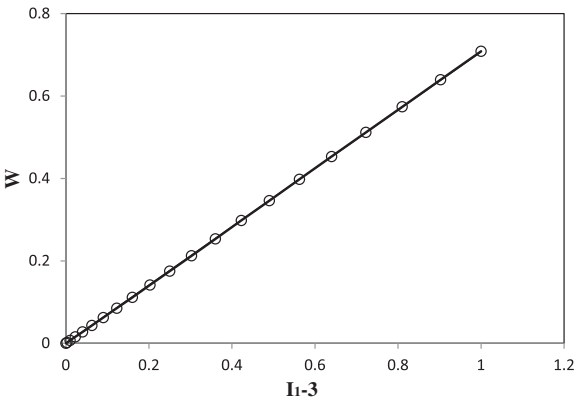

(c) Strain energy $\overline{W}$ vs. $I_1 - 3$ for simple shear simulation

Fig. 21. The average strain energy $\overline{W}$ vs. $I_1 - 3$ curves of the simple "one particle in the centre" unit cell model for three loading cases: uniaxial tension (a), uniaxial compression (b), and simple shear (c).

with this particular type of microstructure under finite deformation, FEM simulations of the unit cell model are performed in ABAQUS for uniaxial tension/compression and simple shear. The particle volume fraction $c = 0.2$ and there are around 20,000 tetrahedral elements and 30,000 nodes in the FEM model. Both the matrix and the particles are modeled as incompressible neo-Hookean materials with $\mu_m = 1$ and $\mu_r = 10$, respectively. In all simulations, PBC is applied to get a good estimate of the real response of the composite and a deformed unit cell is shown in Fig. 20(b). The average strain energy $\overline{W}$ vs. $I_1 - 3$ curves are plotted for three loading cases (Fig. 21). For each loading case, a clear proportional relation between $\overline{W}$ and $I_1 - 3$ can be observed and the effective shear moduli predicted from uniaxial tension/compression and simple shear simulations are $\mu_c = 1.6698$ ($R^2 = 0.9999$, uniaxial tension), 1.8596 ($R^2 = 0.9989$, uniaxial compression) and 1.4150 ($R^2 = 1.0$, simple shear), respectively. The relative difference is about 27.2%, while for the multi-particle RVE models with $(c = 0.2, \mu_r = 10)$ used in the paper, the maximum relative difference between effective shear moduli predicted by different loading cases is well below 1.2%. The effective modulus predicted by the multi-particle RVE models ($c = 0.2$, $\mu_r = 10$) is $\mu_c = 1.4946$. The comparisons between the results from one-particle unit cell model and multi-particle RVE models suggest that, although the effective modulus predicted by the one-particle unit cell model is close to the one predicted by multi-particle RVE models (relative error about 20%), the behavior of the one-particle unit cell model is anisotropic under finite deformation, as determined by its orthotropic microstructure. Furthermore, a one-particle unit cell model cannot capture the characteristics of the stress/strain field in the matrix necking zone, which is critical to the strength investigation of the IPRNC. Hence multi-particle RVE models should be used to obtain realistic response of IPRNC under finite deformation.

5. Concluding remarks

Three-dimensional RVE models are employed to investigate the mechanical behavior of the IPRNC, in which both the matrix and the particle reinforcement are incompressible neo-Hookean materials. To consider different particle volume fractions (i.e., $c = 0.05$, 0.1, 0.2, 0.3), 16 RVE samples (4 for each volume fraction value) with periodic microstructures are created. In each RVE, 27 non-overlapping identical spheres are randomly distributed in a cubic unit. The isotropy of the random distributions of particles in the 16 RVE models is then examined, and the RVE models are meshed for finite element computation. Periodic meshes are generated so that the periodic boundary conditions can be applied during the FEM simulations. The mesh convergence study shows that a standard mesh with about 80,000 elements can obtain accurate result.

To double check the isotropy of the RVE models' mechanical responses, uniaxial tensions and compressions along different directions are simulated for the RVE models and the isotropy of the RVE models is verified directly. The simulation results of the uniaxial tension and compression are consistent, which implies that the small-size RVE models used here are sufficient to obtain accurate responses of the IPRNC. The computed strain energy data suggests that the mechanical response of the IPRNC can be well predicted by an incompressible neo-Hookean model. Material instability is not considered in this paper.

Four different particle/matrix stiffness ratios are studied in the FEM simulations: $\mu_r/\mu_m = \infty$ (i.e., rigid particles), 100, 10, 0.5, to investigate the effect of stiffness contrast between the particle and the matrix. The following four types of finite deformations are simulated: uniaxial tension and compression along coordinate axial directions and random directions, simple shear, and general biaxial deformation. All the simulation results (i.e., RVE with any particle volume fraction, any particle/matrix stiffness ratio and any loading case) show that the average strain energy $\overline{W}$ is proportional to $I_1 - 3$, which suggests that the overall behavior of the IPRNC can be modeled by an incompressible neo-Hookean model. The effective shear moduli μ_c of the IPRNCs are obtained by fitting the strain energy data from the numerical simulation results. Because the dispersion in the values of the obtained moduli is remarkably small in all cases, the numerical results can be considered as a very close approximation to the "exact" effective shear moduli of the IPRNC. They are compared with three theoretical models: the self-consistent estimate, SCE (Castaneda, 1989), the strain amplification estimate for composites with rigid particles, SAE (Bergstrom and Boyce, 1999), and the classical linear elastic three phase model, TPM (Christensen and Lo, 1979). It is found that the TPM provides very accurate approximation to the numerical results (maximum relative difference less than 5.1%) though it is developed for linear elastic PRC. Even though the SCE and the SAE are proposed for neo-Hookean composites, they overestimate the effective shear modulus of the IPRNC when the particle volume fraction $c > 0.1$. In present work, we neglect the viscous behavior of particle reinforced elastomer, which was observed in many experiments. Previous works on viscoelasticity (Tang et al., 2008a,b) can be extended in the strategy presented here to account for the memory of the material.

The numerical approach employed here can be used to study the mechanical responses of other composites (e.g., particle-reinforced composite with matrix of Ogden model) in finite deformation regime. But due to the strong material and geometrical nonlinearity, it is usually much more difficult if not impossible to construct a simple constitutive model to fit the obtained numerical results.

In the numerical simulations, it is usually assumed that the particle fillers will not change the mechanical properties of the matrix. However, many researchers argued that, for elastomers, the fillers may alter the effective crosslinking density in the elastomeric phase and therefore affect the mechanical properties of the matrix (a detailed discussion can be found in Bergstrom and Boyce (1999)). Because of this, the numerical results are not compared with the finite deformation experimental data rarely available in the literature.

We note that mesh of the matrix necking zone between close particles is very challenging and severe deformation localization may happen when the stiffness contrast be-

tween the particle and the matrix is large. Hence convergence is a big issue in our numerical simulation even for RVE models with very refined mesh (e.g., with more than 200,000 elements). For example, it is only possible to reach moderate deformation state for some cases (e.g., $I_1 = 3.06$, or 14% tension for the IPRNC with $(\mu_r = \infty, c = 0.3)$). For much less critical case like the IPRNC with $(\mu_r = 0.5, c = 0.3)$, huge deformation can be reached (i.e., 313% tension or 86% compression). The numerical results show clearly that up to the deformations the FEM simulations can reach (that is, until there is a convergence problem), all the numerical results of $\bar{W}$ and $I_1 - 3$ can be fitted almost exactly using the linear relation suggested by the incompressible neo-Hookean model. Therefore it is safe to conclude that the mechanical behavior of the IPRNC studied here can be well modeled by another incompressible neo-Hookean model within the limit of current FEM software ABAQUS.

Acknowledgement

The financial support from NSFC (No. 11272362, 11272364, China), Ministry of Education (No. 313059, China), the Fundamental Research Funds for the Central Universities (CDJZR112248801, CDJZR12110072, China), State Key Laboratory of Coal Mine Disaster Dynamics and Control (Chongqing University, China), Opening fund of State Key Laboratory of Nonlinear Mechanics (China), and EPSRC (EP/H016619, UK) is greatly appreciated.

References

ABAQUS, 2010. Analysis User's Manual, Version 6.10. SIMULIA Inc.
Avazmohammadi, R., Castaneda, P.P., 2012. Tangent second-order estimates for the large-strain, macroscopic response of particle-reinforced elastomers. J. Elast., 1–45.
Bergstrom, J.S., Boyce, M.C., 1999. Mechanical behavior of particle filled elastomers. Rubber Chem. Technol 72, 633–656.
Castaneda, P.P., 1989. The overall constitutive behavior of nonlinearly elastic composites. Proc. Roy. Soc. A: Math. Phys. Engng. Sci. 422, 147–171.
Chen, C., Lu, T.J., Fleck, N.A., 1999. Effect of imperfections on the yielding of two-dimensional foams. J. Mech. Phys. Solids 47, 2235–2272.
Christensen, R.M., Lo, K.H., 1979. Solutions for effective shear properties in three phase sphere and cylinder models. J. Mech. Phys. Solids 27, 315–330.
Cohen, I., 2004. Simple algebraic approximations for the effective elastic moduli of cubic arrays of spheres. J. Mech. Phys. Solids 52, 2167–2183.
deBotton, G., Hariton, I., Socolsky, E.A., 2006. Neo-Hookean fiber-reinforced composites in finite elasticity. J. Mech. Phys. Solids 54, 533–559.
Drugan, W.J., Willis, J.R., 1996. A micromechanics-based nonlocal constitutive equation and estimates of representative volume element size for elastic composites. J. Mech. Phys. Solids 44, 497–524.
Guo, Z.Y., Caner, F., Peng, X.Q., Moran, B., 2008. On constitutive modelling of porous neo-Hookean composites. J. Mech. Phys. Solids 56, 2338–2357.
Guo, Z.Y., Peng, X.Q., Moran, B., 2006. A composites-based hyperelastic constitutive model for soft tissue with application to the human annulus fibrosus. J. Mech. Phys. Solids 54, 1952–1971.
Guo, Z.Y., Peng, X.Q., Moran, B., 2007. Large deformation response of a hyperelastic fibre reinforced composite: theoretical model and numerical validation. Compos. A: Appl. Sci. Manufact. 38, 1842–1851.
Guth, E., 1945. Theory of filler reinforcement. J. Appl. Phys. 16, 20–25.
Hashin, Z., 1985. Large isotropic elastic-deformation of composites and porous-media. Int. J. Solids Struct. 21, 711–720.
Hashin, Z., Shtrikman, S., 1963. A variational approach to the theory of the elastic behaviour of multiphase materials. J. Mech. Phys. Solids 11, 127–140.
Hill, R., 1965. A self-consistent mechanics of composite materials. J. Mech. Phys. Solids 13, 213–222.
Hill, R., 1972. Constitutive macro-variables for heterogeneous solids at finite strain. Proc. Roy. Soc. Lond. A: Math. Phys. Sci. 326, 131–147.
Hohe, J., Becker, W., 2003. Effective mechanical behavior of hyperelastic honeycombs and two-dimensional model foams at finite strain. Int. J. Mech. Sci. 45, 891–913.
Imam, A., Johnson, G.C., Ferrari, M., 1995. Determination of the overall moduli in second-order incompressible elasticity. J. Mech. Phys. Solids 43, 1087–1104.
Kerner, E.H., 1956. The elastic and thermo-elastic properties of composite media. Proc. Phys. Soc. Lond. B 69, 808.
Khisaeva, Z.F., Ostoja-Starzewski, M., 2006. On the size of RVE in finite elasticity of random composites. J. Elast. 85, 153–173.
Kouznetesova, V., 2002. Computational Homogenization for the Multi-scale Analysis of Multi-phase Materials. Eindhoven University of Technology.
Lopez-Pamies, O., 2010. An exact result for the macroscopic response of particle-reinforced neo-Hookean solids. J. Appl. Mech. 77, 021016.
Michel, J.C., Moulinec, H., Suquet, P., 1999. Effective properties of composite materials with periodic microstructure: a computational approach. Comput. Method Appl. Mech. Engrg. 172, 109–143.
Miehe, C., Schroder, J., Becker, M., 2002. Computational homogenization analysis in finite elasticity: material and structural instabilities on the micro- and macro-scales of periodic composites and their interaction. Comput. Method Appl. Mech. Engrg. 191, 4971–5005.
Moraleda, J., Segurado, J., Llorca, J., 2007. Finite deformation of porous elastomers: a computational micromechanics approach. Phil. Mag. 87, 5607–5627.
Moraleda, J., Segurado, J., Llorca, J., 2009. Finite deformation of incompressible fiber-reinforced elastomers: a computational micromechanics approach. J. Mech. Phys. Solids 57, 1596–1613.
Ogden, R.W., 1974. Overall moduli of nonlinear elastic composite-materials. J. Mech. Phys. Solids 22, 541–553.
Segurado, J., Llorca, J., 2002. A numerical approximation to the elastic properties of sphere-reinforced composites. J. Mech. Phys. Solids 50, 2107–2121.
Segurado, J., Llorca, J., 2005. A computational micromechanics study of the effect of interface decohesion on the mechanical behavior of composites. Acta Mater. 53, 4931–4942.
Segurado, J., Llorca, J., 2006. Computational micromechanics of composites: the effect of particle spatial distribution. Mech. Mater. 38, 873–883.
Tang, S., Greene, M.S., Liu, W.K., 2012a. A renormalization approach to model interaction in microstructured solids: application to porous elastomer. Comput. Method Appl. Meth. 217, 213–225.
Tang, S., Greene, M.S., Liu, W.K., 2012b. Two-scale mechanism-based theory of nonlinear viscoelasticity. J. Mech. Phys. Solids 60, 199–226.
Tang, S., Guo, T.F., Cheng, L., 2008a. Mode mixity and nonlinear viscous effects on toughness of interfaces. Int. J. Solids Struct. 45, 2493–2511.
Tang, S., Guo, T.F., Cheng, L., 2008b. Rate effects on toughness in elastic nonlinear viscous solids. J. Mech. Phys. Solids 56, 974–992.
Torquato, S., 1998. Effective stiffness tensor of composite media: II. Applications to isotropic dispersions. J. Mech. Phys. Solids 46, 1411–1440.